# Characterizing the Spatial Morphologies and Temporal Dynamics of Biologically Inspired Multicomponent Systems

Ifunanya Nwogbaga

Department of Chemical and Biological Engineering
Class of 2018

Submitted to the
Program in Applied and Computational Mathematics
Princeton University
in partial fulfillment of the requirements of
Undergraduate Independent Work.

Final Report

30 April 2018

Advisor:
Professor Mikko Haataja

38 pages

© Copyright by Ifunanya Nwogbaga, 2019.
All Rights Reserved

This final report represents my own work in accordance with University regulations.

# Acknowledgements

I want to thank my advisor, Professor Mikko Haataja, for mentoring me and guiding me and allowing me to join him in this cool research project. I would also like to thank Professor Andrej Košmrlj for mentoring me throughout the process and providing valuable insight at each point. Lastly, I would like to thank Dr. Sheng Mao, who really helped and guided me throughout every little step. Sheng's mentorship has been integral in my development not only as a scientist, but also as a person, a person who can ask critical questions and figure out how to address those questions. These are skills that will be valuable to me not just in academia, but in real life as well.

# Abstract

The phrase "liquid-liquid phase separation" has been prevalent in the field of biophysics over the last several years due to discoveries that have been made in cells and other biological systems. These discoveries have revealed that biological systems undergo thermodynamic phase separations, similar to how oil and water phase separate when mixed together. For instance, scientists have observed organelles in cells, such as P. granules, or proteins in the brain forming aggregates. The formation of aggregates gives rise to different phases, each phase having a unique chemical composition and intereacting with other phases like immiscible liquids. This occurs passively, as if the system was tending towards thermodynamic equilibrium. This is interesting as biological systems are not at equilibrium. In this report, we attempt to illuminate the spatial and temporal dynamics of phase equilibria for ternary and quaternary systems, observing the kinetics and comparing to what we predict thermodynamically. We discover that the kinetic results often differ from the thermodynamic pedictions. This reveals that the kinetics of a mixture can only be fully understood from the full temporal evolution of a system. However, finding a method for generalizing our results and understanding how phase equilibria evolves in higher order systems still remain a challenge.

# Contents

Acknowledgements . . . . . iii
Abstract . . . . . iv
List of Tables . . . . . vi
List of Figures . . . . . vii

**1 Introduction** **1**
1.1 Challenges in Multicomponent Systems . . . . . 1
1.2 Objectives and Outline . . . . . 2
1.3 Experimental Evidence . . . . . 3
1.4 Thermodynamics Background . . . . . 3
1.5 Current Models . . . . . 6

**2 Numerical Methods** **7**
2.1 Finite Element Method (FEM) . . . . . 7
2.2 Implementation in FEniCS . . . . . 9
2.3 Solving the Cahn-Hilliard-Cook Equation . . . . . 13
2.4 Numerical Analysis of the Cahn-Hilliard-Cook Equation . . . . . 16

**3 Results and Discussion** **18**
3.1 Ternary System . . . . . 18
3.1.1 Thermodynamic Results . . . . . 18
3.1.2 Kinetic Results . . . . . 19
3.1.3 Stability Analysis . . . . . 22
3.2 Quaternary System . . . . . 24

**4 Conclusions and Future Work** **28**

# List of Tables

3.1 3-Component System Parameter Values . . . . . 18
3.2 4-Component System Parameter Values . . . . . 25

# List of Figures


1.1 Binary Phase Diagram . . . . . 5
1.2 Ternary Phase Diagram Example . . . . . 6

2.1 Wave Equation Output 1 . . . . . 11
2.2 Wave Equation Output 2 . . . . . 14

3.1 Thermodynamic Ternary Phase Diagram . . . . . 19
3.2 RGB Reference Triangles . . . . . 20
3.3 Thermodynamic Ternary Phase Diagram Interior Points . . . . . 20
3.4 Kinetic Ternary Phase Diagram . . . . . 22
3.5 Phase Diagrams . . . . . 23
3.6 Eigenvalue Kinetic Ternary Phase Diagram . . . . . 24
3.7 Quaternary: Equal Interactions, Equimolar . . . . . 25
3.8 Quaternary: Unequal Interactions Cases 2 and 3, Equimolar . . . . . 26
3.9 Quaternary: Unequal Interactions Case 4, Equimolar . . . . . 27

# Chapter 1

# Introduction

## 1.1 Challenges in Multicomponent Systems

Multicomponent systems are mixtures that contain multiple pure substances or components [1]. A common example is the binary mixture of oil and water. Oil and water are two immiscible liquids that possess different compositions. Multicomponent mixtures often exhibit dynamic phase behavior, even when the number of components is small. For instance, oil and water separate into two separate phases upon mixing, a phenomenon known as a phase transition, when new phases form or when phases coalesce.. Phases are defined as mechanically separable regions possessing different compositions [2]. Since multicomponent systems have many applications in industry, the rise of the study of their phase behavior has increased drastically over the past several decades. For instance, in metallurgy, the development of multicomponent metal alloys has required detailed understanding of both the microstructure and the molecular organization of the mixtures. This understanding subsequently reveals the number and types of phases that the system exhibits when certain key metals used for manufacturing materials, such as nickel (Ni) or iron (Fe), have low or high concentrations [3]. Study and development of metal alloys and their phase behavior has allowed researchers and industrial workers to create robust metal mixtures that have a wide range of applications, such as more bio-compatible orthopedics [4].

More recently, cells and other biological systems are being studied as multicomponent systems. For example, membraneless organelles segregate into different compartments of the cell, undergoing phase transitions. This segregation is crucial for controlling cellular organization [5]. Another example of phase transitions in biology

has emerged in the study of neurodegenerative diseases such as Amyotrophic Lateral Sclerosis (ALS). RNA-binding proteins fused in sarcoma (FUS) transition into various aggregate states that behave as phase separated liquids. Unfortunately, these aggregate states become neurotoxic, adding to a cascade of other complications that lead to ALS. Other neurodegenerative diseases are also believed to be related to phase transitions and aggregation of proteins [6].

The presence of multicomponent systems in a wide range of applications, from metal production to medicine, has raised questions on how to quantify the phase behavior and dynamics of multicomponent systems. Unfortunately, understanding the dynamics of an arbitrarily large system of N components is highly nontrivial. It requires one to simultaneously solve many differential equations relating to different properties of the system, such as the free energy, using first principles from thermodynamics and statistical mechanics [7]. Nonetheless, people still study multicomponent systems by starting from systems with only N = 2 (binary) or N = 3 components (ternary). Studies of these small component systems still provide beneficial insight for how higher order systems, mixtures with several components, behave. The kinetics and thermodynamics of binary systems are well documented [8, 9, 10, 11, 12], though detailed knowledge of ternary and higher order systems is not as well developed. Thus, in this report, ternary and quaternary systems (N = 4) were studied and characterized.

## 1.2 Objectives and Outline

1. Understand the morphologies for ternary and quaternary systems in two dimensions.
2. Construct thermodynamic and kinetic phase triangles for the systems of choice.
3. Explore and analyze the dynamics of the ternary mixture by varying the initial conditions (starting compositions) and interaction parameters between each component.
4. Study equimolar quaternary mixture dynamics by varying the interaction parameters.
5. Attempt to formulate a method for generalizing key results for N-component systems.

The rest of this report will be as follows: the remainder of Chapter 1 will contain more background on multicomponent systems, the theory and models used to study them, and the experimental evidence used to propel research in this field. Chapter 2 will discuss the numerical methods used to solve Model B, the main equation of interest for our systems that we are studying. Chapter 3 will discuss the key results obtained from our studies, and Chapter 4 will briefly summarize what we have learned and how that relates back to the main problem at hand and what others have done in the past. Afterwards, directions for future work will addressed.

## 1.3 Experimental Evidence

Many multicomponent systems with hundreds or thousands of components only give rise to few unqiue phases, often fewer than 10. This is especially true in biology. For instance, liquid-liquid phase separation has been shown in cells, facilitating the packing of membraneless organelles. Reference [13] has shown that ribosomes, DNA, and RNA form spherical packings in biological cells, often showing only three phases and effectively very few components, even though there are technically hundreds of components. The study of multicomponent systems is especially challenging and interesting since a mixture of hundreds or thousands of components can behave like a system with effectively much fewer components. Thus, this provides evidence and support for studying smaller mixtures like ternary and quaternary systems, as they can provide insight for higher order systems, mixtures with many more components.

## 1.4 Thermodynamics Background

The amount of each component is often denoted by a concentration, which could be defined on a mass or molar basis. When the dynamics of multicomponent mixtures are studied, the important questions often are concerned with how many phases exist under a prescribed set of parameters and what types of morphologies are observed, i.e. what spatial configurations do the different components visit? This is determined by the thermodynamics of the system. If the system is closed, it will obey the first and second laws of thermodynamics, which state that energy is conserved and the entropy of the system is always increasing [14]. These laws are important, as energy and entropy are often in competition with each other. Systems generally try to minimize their free energy, often defined as the system's capacity to do work [15] while

maximizing their entropy. Depending on the compositions of the different components present and the component's tendencies to interact or repel each other, sometimes energy dominates and other times entropy dominates. For instance, in a regular solution, a system discretized into grids where each grid contains at most one molecule [16], the free energy density of a regular polymer solution, as characterized by the Flory-Huggins theory [17, 18], is given by

$$f(c) = \sum_{i=1}^{N} c_i \ln(c_i) + \sum_{i<j} \chi_{ij} c_i c_j, \tag{1.1}$$

where the set of $\{c_i\}$ are the concentrations of each of the N components in the solution, constrained by $\sum_i c_i = 1$, and $\chi_{ij}$ is the interaction energy between components $c_i$ and $c_j$. The free energy is given in units of $k_B T$, where $k_B$ is Boltzmann's constant and T is absolute temperature. The first term in the Equation (1.1) is the entropy dominated term and the second term is energy dominated. For illustration purposes, consider a two-component system. When the interaction energy, $\chi_{12}$ is small, the entropy term dominates. Under entropy-dominating conditions, the system will prefer to be well mixed and will stabley exist as one phase when equilibrium is reached. Conversely, when the interaction energy is large enough, the energy term dominates, allowing the system to separate into two different phases even though it is usually not entropically favorable for the molecules of the system to self-segregrate [16]. This is illustrated in the bottom plot of Figure 1.1. Competition between energy and entropy also give rise to locally stable or unstable regions of the system, conditions that are determined by the second derivative of the free energy. For instance, considering a two-component system, the magnitude of the interaction energy will determine whether the second derivative of the free energy density will be positive or negative. A positive second derivative means that the system must raise its free energy to move to another composition, so the system is stable. Stable systems are situated in the binodal region for two component systems. When the second derivative is negative, the system lowers its free energy by moving to a different composition, meaning that the system is inherently unstable. Unstable systems are situated in the spinodal region [16].

The binodal and spinodal regions can be visualized in phase diagrams. Phase diagrams are graphs that depict how thermodynamically distinct phases can coexist, depending on how many components are in the system. Construction of these systems is heavily dependent on the free energy of the system and entropy. As an example,

the top plot of Figure 1.1 shows the phase diagram for a binary system. Depicted is the free energy of the system as it changes as a function of the concentration of one of the components, with the binodal and spinodal regions labeled. The binodal region corresponds to the conditions where two phases can coexist, where the system free energy is stable. This stability is visualized in the local minima of the graph, where the second derivative is positive. The spinodal region corresponds to the region where one phase exists, but small fluctuations will cause the system to phase separate. This instability is visualized in the local maximum of the graph, where the second derivative is negative.

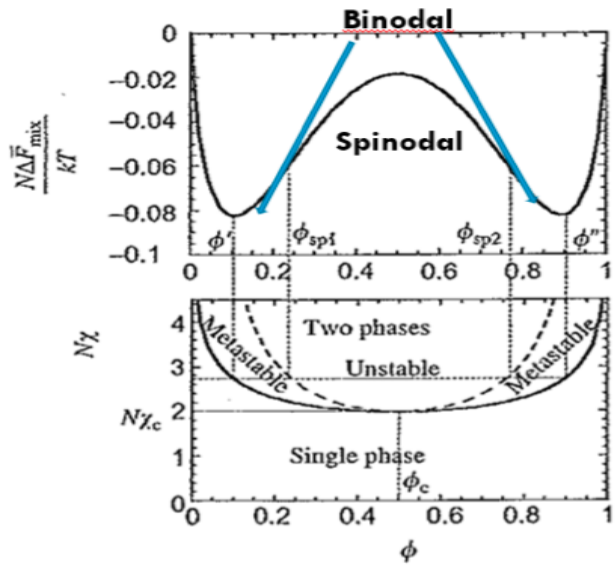


**Figure 1.1:** Binary Phase Diagram. Top: On x axis is the concentration of one of the components. On the y axis is the normalized free energy. Bottom: On the y axis is the value of interaction energy, $\chi$. Figure adapted from Reference [19].

For ternary and quaternary systems, phase diagrams in the form of triangles and triangular pyramids respectively delineate how phase equilibria is related to composition of the different components [20]. An example of a ternary phase diagram is shown in Figure 1.2. The different colored regions correspond conditions where the system exists in a one-phase (black), two-phase (blue), or three-phase (white) state, depending on the concentration of all three components, A, B, and C. More details on how these diagrams are read will be discussed further in Chapter 3.

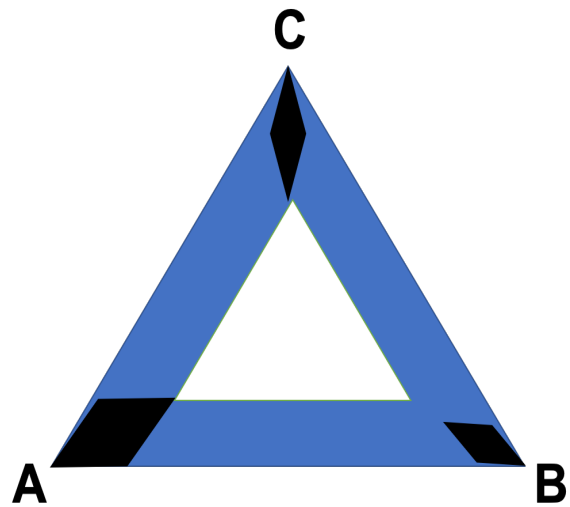


**Figure 1.2:** Example of a ternary phase diagram.

## 1.5 Current Models

Several models have been proposed for the dynamics of multicomponent systems. For instance, the stochastic Allen-Cahn equation, often referred to as Model A, describes the dynamics of the system with a nonconserved parameter that is not uniquely determined by concentration, temperature, pressure, etc. [21]

$$\frac{\partial \phi}{\partial t} = -\Gamma \frac{\delta F[\phi]}{\delta \phi} + \xi_A(\vec{\mathbf{r}}, t), \tag{1.2}$$

where the nonconserved parameter, $\phi$, often represents the phase of the system; $\Gamma$ is the mobility constant; $\frac{\delta F[\phi]}{\delta \phi}$ is the free energy functional of the system; $\xi_A$ is a stochastic term with $\langle \xi_A \rangle = 0$ and $\langle \xi_A(\vec{\mathbf{r}}_1, t_1)\xi_A(\vec{\mathbf{r}}_2, t_2)\rangle = 2\Gamma k_B T \delta(\vec{\mathbf{r}}_1 - \vec{\mathbf{r}}_2)\delta(t_1 - t_2)$; $k_B$ is Boltzmann's constant; $T$ is the absolute temperature in Kelvin.

Similar to Model A, Model B, also known as the stochastic Cahn-Hilliard-Cook equation, is a generalized diffusion equation that uses a locally conserved parameter, such as concentration $c$, to describe the dynamics of the system [21]:

$$\frac{\partial c}{\partial t} = \Gamma \nabla^2 \frac{\delta F[c, \nabla c]}{\delta c} + \xi_B(\vec{\mathbf{r}}, t), \tag{1.3}$$

where $\langle \xi_B \rangle = 0$ and $\langle \xi_B(\vec{\mathbf{r}}_1, t_1)\xi_B(\vec{\mathbf{r}}_2, t_2)\rangle = -2\Gamma k_B T \nabla^2 \delta(\vec{\mathbf{r}}_1 - \vec{\mathbf{r}}_2)\delta(t_1 - t_2)$. Since $c$ is locally conserved, it follows Fick's second law: $\frac{\partial c}{\partial t} = -\nabla \cdot \vec{\mathbf{J}}$, where $\vec{\mathbf{J}} = \nabla \frac{\delta F[c, \nabla c]}{\delta c}$. For this report, Model B was utilized for studying 3- and 4-component systems.

# Chapter 2

# Numerical Methods

## 2.1 Finite Element Method (FEM)

Quantitative analysis of multicomponent systems and phase transitions often require solving partial differential equations (PDEs). One common numerical method for solving PDEs is finite differences [22]. However, this method has its flaws as it is prone to numcerial instability. Thus, we used a general, more robust tool for finding numerical solutions to PDEs known as Galerkin's FEM in this report to solve Model B [23]. FEM was implemented in the open-source computing platform FEniCS (**F**inite **E**lement **C**omputing **S**oftware) [24], which provides a means to solve PDEs efficiently and effectively using FEM utilizing Python and C++ interfaces.

Before Model B was solved, we solved a few easier equations first to understand how FEM is implemented. One of our test cases was the wave equation [25]

$$\frac{\partial^2 u}{\partial t^2} = c^2 \nabla^2 u, \quad u(0,t) = u_0, \quad \frac{\partial u(0,t)}{\partial t} = 0, \tag{2.1}$$

where $u$ is the spatial displacement of the wave and $c$ is the speed of light, prescribed a value of 1 for simplicity, and $u_0$ is the initial displacement. In order to solve the wave equation, it was broken down into two coupled differential equations:

$$\frac{\partial u}{\partial t} = v, \quad \frac{\partial v}{\partial t} = \nabla^2 u, \quad u(0,t) = u_0, \quad v(0,t) = 0, \tag{2.2}$$

The time derivatives were discretized and solved implicitly using the Crank-Nicholson

method [26]:

$$\frac{\partial u}{\partial t} \approx \frac{u^{n+1} - u^n}{\Delta t} = \frac{v^{n+1} + v^n}{2}, \quad \frac{\partial v}{\partial t} \approx \frac{v^{n+1} - v^n}{\Delta t} = \nabla^2 \left( \frac{u^{n+1} + u^n}{2} \right). \tag{2.3}$$

Here, $u^{n+1}$ and $v^{n+1}$ are the unknown functions that we wish to solve. These are denoted as *trial functions*. On the other hand, $u^n$ and $v^n$ are functions that we have already solved for. These are conveniently coined the *known functions*. The Laplacian term, $\nabla^2$, is handled using Galerkin's FEM. We first start by formulating the wave equation in variational form [23, 24]. In order to turn the wave equation into its variational form, we multiply each of the two coupled equations by a *test function*, $u_{test}$ or $v_{test}$, integrate the resulting equations over the domain $\Omega$ that the wave equation is defined in, and perform integration by parts on the Laplacian terms. The formulation is outlined below:

First, isolate the trial functions to one side:

$$u^{n+1} = \frac{\Delta t}{2}(v^{n+1} + v^n) + u^n, \quad v^{n+1} = \frac{\Delta t}{2}\nabla^2(u^{n+1} + u^n) + v^n. \tag{2.4}$$

Then multiply by the test functions and integrate over $\Omega$:

$$\int_\Omega u^{n+1} \cdot u_{test}\, dx = \frac{\Delta t}{2} \int_\Omega [(v^{n+1} + v^n) + u^n] \cdot u_{test}\, dx, \tag{2.5}$$

$$\int_\Omega v^{n+1} \cdot v_{test}\, dx = \frac{\Delta t}{2} \int_\Omega [\nabla^2(u^{n+1} + u^n) + v^n] \cdot v_{test}\, dx. \tag{2.6}$$

Equation (2.6) can be simplified further. First, we know that for two functions $u$ and $v$, $\nabla \cdot (v\nabla u) = \nabla v \cdot \nabla u + v\nabla^2 u \quad \Rightarrow \quad v\nabla^2 u = -\nabla v \cdot \nabla u + \nabla \cdot (v\nabla u)$. Second, once we integrate, the divergence term $\nabla \cdot (v\nabla u)$ can be simplified further using the divergence theorem, which states [27]:

$$\int_\Omega \nabla \cdot (v\nabla u)\, dx = \int_{\partial\Omega} (v\nabla u) \cdot \hat{\mathbf{n}}\, ds = \int_{\partial\Omega} \frac{\partial u}{\partial n} v\, ds, \tag{2.7}$$

where $\nabla u \cdot \hat{\mathbf{n}} \equiv \frac{\partial u}{\partial n}$. As the boundary $\partial\Omega$ gets larger, the term in Equation (2.7) goes to zero. Hence, we can rewrite Equation (2.6) as:

$$\int_\Omega v^{n+1} \cdot v_{test}\, dx = \frac{\Delta t}{2} \int_\Omega [-\nabla(u^{n+1} + u^n) \cdot \nabla v_{test} + v^n \cdot v_{test}]\, dx. \tag{2.8}$$

The left-hand sides of Equations (2.5) and (2.8) are known as the bilinear forms, while the right-hand sides are known as the linear forms. Breaking down the equations into these two forms is essential to implementing FEM in FEniCS.

## 2.2 Implementation in FEniCS

Below is how the code was implemented in Python. Original code was developed by Dr. Sheng Mao at Princeton University following the guidelines for FEniCS for similar equations [24]:

```
# import necessary library
from fenics import *
# this line is to set the plotting
backend of fenics to matplotlib to
avoid error messages
parameters ['plotting_backend'] = 'matplotlib'
# extra features that might be used from matplotlib
from matplotlib import pyplot as plt
# set notebook to show figures by default
%matplotlib inline
# ohter standard libraries
import numpy as np

# build mesh and function space
# 1D: UnitIntervalMesh, 2D: UnitSquareMesh, 3D: UnitCubeMesh
mesh = UnitIntervalMesh(20)
# build elements
ele  = FiniteElement("CG", mesh.ufl_cell(), 1)
# mixed function space
ME   = FunctionSpace(mesh, MixedElement([ele, ele]))
# our functions (u,v) stored in w
w     = TrialFunction(ME) # unknowns
```

```
wPrev = Function(ME)      # previous step (known function)
wTest = TestFunction(ME)  # arbitraty test functions (no need to know)
# split them here
u, v         = split(w)
uPrev, vPrev = split(wPrev)
uTest, vTest = split(wTest)

# exact solution, initial and boundary conditions
alpha = 1.3
beta  = 1.0
D     = 1.0
t     = 0.0
dt    = 0.01
steps = 50

# Define exact solution
wExact = Expression(('sin(pi*x[0])*cos(pi*t)', '-pi*sin(pi*x[0])*sin(pi*t)'),
degree=2, pi=pi, t=0)

# initial condition
wPrev  = interpolate(wExact, ME)

# boundary condition
def boundary(x, on_boundary):
return on_boundary

bc = DirichletBC(ME, wExact, boundary)

"""
this is important. so from the plots below we know that we need to split the
```

```
function wPrev again to make sure that uPrev and vPrev are not assigned as 0,
otherwise the initial condition will be wiped out!!!
"""
# before split
plot(uPrev)
plt.title('Before Splitting wPrev second time')
# after split
uPrev, vPrev = split(wPrev)
plt.figure()
plot(uPrev)
plt.title('After Splitting wPrev second time')
```

Output of code in Figure 2.1.

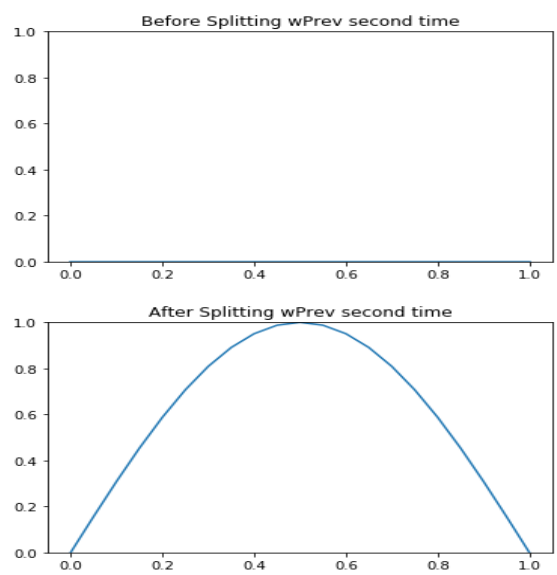


**Figure 2.1:** Output of using FEniCS to solve the wave equation. This output is to check that initial conditions are as prescribed before moving forward.

```
# weak formulation
# source term
f  = Constant(0.0)
# Equation one: u = uPrev + 0.5*(v+vPrev)*dt
F1 = u*uTest*dx - uPrev*uTest*dx - 0.5*dt*(v+vPrev)*uTest*dx
```

```
# Equation two: v = vPrev + 0.5*(acc+accPrev)*dt
accPrev = f*vTest - D*inner(grad(uPrev), grad(vTest))
acc     = f*vTest - D*inner(grad(u), grad(vTest))
F2      = v*vTest*dx - vPrev*vTest*dx - 0.5*dt*(acc+accPrev)*dx
# assemble the linear system of equations
F  = F1 + F2
# split the left and right hand sides
a, L = lhs(F), rhs(F)
# solution to be stored in w
w = Function(ME)

# looping in time to obtain time-dependent solution
# steps: num of time steps
# dt: time step
# all defined at the beginning of the code
for step in range(steps):
# advance in one time step
t += dt
step += 1
wExact.t = t   # this also updates the boundary condition bc
solve(a==L, w, bc)
# update previous step
wPrev.vector()[:] = w.vector()

## compare with exact solution
wExactFunc = interpolate(wExact, ME)
## "%" means remainder. so every 10 steps we output figures
if step%10 ==1:
# figure one, the u field
plt.figure()
```

```
plot(w.split()[0])
# compare with exact solution
plot(wExactFunc.split()[0])
# set the ylimit of the 1D plot
plt.ylim(-1,1)
# figure two, the v field
plt.figure()
plot(w.split()[1])
# compare with exact solution
plot(wExactFunc.split()[1])
# set the ylimit of the 1D plot
plt.ylim(-4,4)
# calculate error and print it out on screen
error = (w.vector().array() - wExactFunc.vector().array()).max()
# %f means floating number, %g means scientific notation,
.3 means three decimals
print ('t = %.3f, error = %.3g' % (t, error))
```

Below in Figure 2.2 are selected outputs of the wave equation solution in 1-dimension. As one can see, the wave starts flat, rises, then descends. This pattern continues for all time steps that this simple simulation was run. Other simple test cases were used but the wave equation was the most simple and representative case illustrating how the more complicated Model B will be solved later.

## 2.3 Solving the Cahn-Hilliard-Cook Equation

Model B without the stochastic term is given by

$$\frac{\partial c}{\partial t} = \Gamma \nabla^2 \frac{\delta F[c, \nabla c]}{\delta c}. \tag{2.9}$$

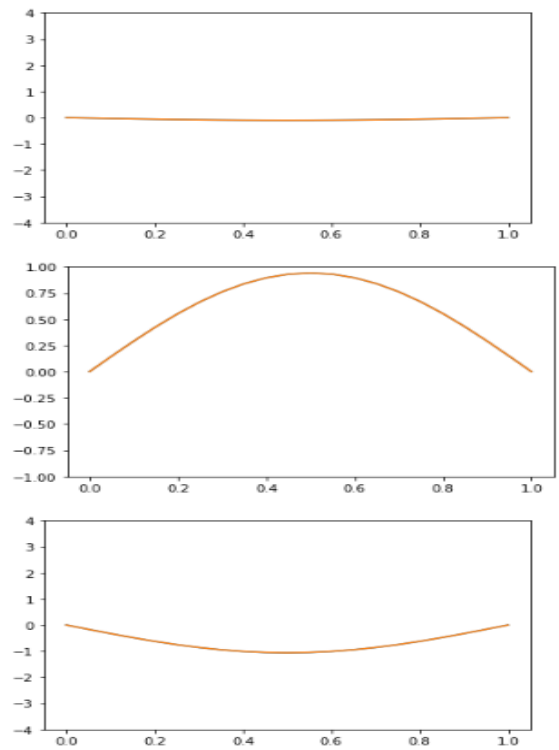


**Figure 2.2:** Output of using FEniCS to solve the wave equation. This output shows evolving standing wave for three subsequent time steps.

Our free energy functional, $F$, is defined as [28]

$$F[c, \nabla c] = \iiint_V (f(c) + \kappa(\nabla c)^2)\, dV, \tag{2.10}$$

where $f(c)$ is the free energy density and $\kappa$ is the composition gradient energy. The variational derivative of the free energy functional can be obtained from the definition of the differential of the free energy function $dF$:

$$dF = \iiint_V dV \left( \left.\frac{\delta F[c, \nabla c]}{\delta c}\right|_{c_0} \delta c + \left.\frac{\delta F[c, \nabla c]}{\delta(\nabla c)}\right|_{c_0} \delta(\nabla c) \right), \tag{2.11}$$

where the free energy variational derivative is evaluated at a certain concentration, $c_0$. Here, we assume that there is no perturbation in the first spatial derivative, making $\delta(\nabla c) = 0$ and removing the second term in Equation (2.11).

To solve Equation (2.11), we must first rewrite it, understanding that the differ-

ential $dF$ is simply the change in the free energy functional [29]:

$$dF = F[c + \delta c, \nabla c] - F[c, \nabla c], \tag{2.12}$$

where $\delta c$ is assumed to be a small perturbation and $F[c + \delta c, \nabla c]$ is defined as

$$F[c + \delta c, \nabla c] = \iiint_V (f(c + \delta c) + \kappa(\nabla(c + \delta c))^2)\, dV. \tag{2.13}$$

Having a small perturbation allows use to perform a Taylor expansion of the free energy density, $f(c + \delta c)$, and keep the first order term [29]:

$$F[c + \delta c, \nabla c] \approx \iiint_V \left( f(c) + \left.\frac{\partial f}{\partial c}\right|_{c_0} \delta c + \kappa[(\nabla c)^2 + (\nabla \delta c)^2 + 2(\nabla c) \cdot (\nabla \delta c)] \right) dV. \tag{2.14}$$

Again, since $\delta c$ is small, $(\nabla \delta c)^2$ is negligible. We can simplify Equation (2.14) even further, however. Given two equations, $h$ and $g$, we can utilize the mathematical identity: $\nabla h \cdot \nabla g = \nabla \cdot (h \nabla g) - h \nabla^2 g$. If we allow $h = \delta c$ and $g = c$, we can utilize the identity in Equation (2.14):

$$F[c + \delta c, \nabla c] \approx \iiint_V \left( f(c) + \left.\frac{\partial f}{\partial c}\right|_{c_0} \delta c + \kappa(\nabla c)^2 + 2\kappa[\nabla \cdot (\delta c \nabla c) - \delta c \nabla^2 c] \right) dV. \tag{2.15}$$

Here, the $\nabla \cdot (\delta c \nabla c)$ term goes to zero thanks to the divergence theorem again [27], which states that

$$\iiint_V \nabla \cdot (\delta c \nabla c)\, dV = \iint_S (\delta c \nabla c) \cdot \hat{\mathbf{n}}\, dS, \tag{2.16}$$

which tends to zero and the surface of integration becomes arbitrarily large. At last, we arrive at the final form of $F[c + \delta c, \nabla c]$:

$$F[c + \delta c, \nabla c] \approx \iiint_V \left( f(c) + \left.\frac{\partial f}{\partial c}\right|_{c_0} \delta c + \kappa(\nabla c)^2 - 2\kappa \delta c \nabla^2 c \right) dV. \tag{2.17}$$

Now we can evaluate $dF$ as

$$dF = \iiint_V dV \left( \left.\frac{\partial f}{\partial c}\right|_{c_0} - 2\kappa \nabla^2 c \right) \delta c = \iiint_V dV \left.\frac{\delta F[c, \nabla c]}{\delta c}\right|_{c_0} \delta c. \tag{2.18}$$

By inspection, we retrieve our equation for the variational derivative:

$$\frac{\delta F[c, \nabla c]}{\delta c} = \frac{\partial f}{\partial c} - 2\kappa \nabla^2 c. \tag{2.19}$$

The exact form of the free energy density will determine the form the variational derivative will take. For this report, the regular solution model [28] for the free energy density was used for $N = 3$ and $N = 4$ component systems with an added term to account for interfacial energy between different components:

$$f(c) = \sum_{i=1}^{N} c_i \ln(c_i) + \sum_{i<j} \chi_{ij} c_i c_j - \frac{1}{2}\lambda^2 \sum_{i<j} \chi_{ij} \nabla c_i \cdot \nabla c_j, \tag{2.20}$$

where $c$ is a vector of $N-1$ independent concentrations, defined as $c \equiv \{c_1, c_2, .., c_{N-1}\}$ and $\sum_{i=1}^{N} c_i = 1$; $\lambda$ is defined as [28]:

$$\gamma_{ab} = \lambda \int_0^1 \sqrt{2\kappa \Delta f_0} d\phi, \tag{2.21}$$

with $\kappa$ defined as [28]

$$\kappa = -\sum_{i<j} \chi_{ij} (c_i^a - c_i^b)(c_j^a - c_j^b). \tag{2.22}$$

Here, $\gamma_{ab}$ is simply the surface tension and is used as a means to calculate $\lambda$ for a system; $\Delta f_0$ is additional free energy that must be accounted for at the interface between two components; $\phi$ denotes a general phase while $a$ and $b$ denote phases that are in contact.

## 2.4 Numerical Analysis of the Cahn-Hilliard-Cook Equation

Our next main challenge is numerical solving Model B. This was done using finite element method on the software package FEniCS. In order to solve Model B, it was broken into two coupled differential equations and solved in the same manner that the wave equation from Equation (2.1) was solved:

$$\frac{\partial c}{\partial t} = \Gamma \nabla^2 \mu, \tag{2.23}$$

$$\mu \equiv \frac{\delta F[c, \nabla c]}{\delta c} = \frac{\partial f}{\partial c} - 2\kappa \nabla^2 c. \tag{2.24}$$

The time derivative is discretized and solved implicitly using the Crank-Nicholson method as well [26]:

$$\frac{\partial c}{\partial t} \approx \frac{c^{n+1} - c^n}{\Delta t} = \frac{1}{2}(\mu^{n+1} + \mu^n). \tag{2.25}$$

The simulations were done on a 2-dimensional grid that was 96x96 in size and the test functions were denoted by $c_{test}$ and $\mu_{test}$. Full code was fully developed and implemented by Dr. Sheng Mao of Princeton University. The code (omitted here) was adapted for this research project.

# Chapter 3

# Results and Discussion

## 3.1 Ternary System

For the 3-component system, the free energy density took the form

$$f(c_1, c_2, c_3) = \sum_{i=1}^{3} c_i \ln(c_i) + \sum_{i<j} \chi_{ij} c_i c_j - \frac{1}{2}\lambda^2 \sum_{i<j} \chi_{ij} \nabla c_i \cdot \nabla c_j, \tag{3.1}$$

where $c_1 + c_2 + c_3 = 1$. Table 3.1 contains the values of the parameters studied:

**Table 3.1:** Values for all the interaction energies and interfacial energies for a 3-component system.

| **Parameter** | **Value** |
|---|---|
| $\chi_{12}$ | 2.5 |
| $\chi_{13}$ | 3.0 |
| $\chi_{23}$ | 3.5 |
| $\lambda$ | $5{\cdot}10^{-5}$ |

### 3.1.1 Thermodynamic Results

For this 3-component system, we know that it produces a thermodynamic ternary phase diagram, as shown in Figure 3.1. The formulation of this phase diagram is detailed in Reference [30] but the method is briefly outlined in this report. The phase diagram was constructed by taking the convex hull of the characteristic functions of this heterogeneous ternary system, such as functions that carry information about the internal energy and entropy. These characteristic functions have a special property:

functions over intensive variables like temperature are convex. Meanwhile, functions of extensive variables like entropy are concave (negative of a convex function) [30].

The convex hull of a set $\Lambda$ of points defined in an affine space over $\mathbb{R}$ is the smallest convex set that contains $\Lambda$ [31]. A convex set, $\zeta$, is defined as a subset of an affine space with the property that any convex combination of any two elements, $x$ and $y$, will also belong in the set, $\zeta$. In other words, $\forall\ \alpha \in[0,1]$, if $\{x, y\}\in \zeta$, then $\alpha x+(1-\alpha)y \in \zeta$ [31]. Knowing what a convex set is, a convex function, $f$, is one that is defined on a convex set, $\zeta$, with the following property: $\forall\ \alpha \in[0,1]$, and $\forall\ \{x, y\}\in \zeta$, $f(\alpha x+(1-\alpha)y) \leq \alpha f(x)+(1-\alpha)f(y)$ [31]. These concepts from convex analysis were utilized with thermodynamics to used to construct these triangles. Understanding

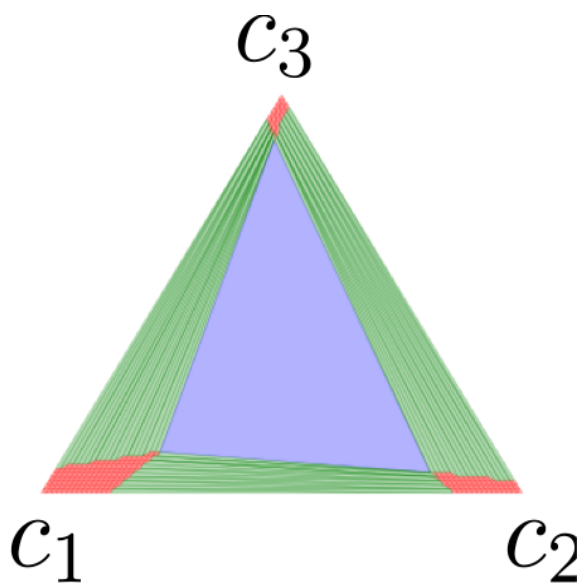


**Figure 3.1:** Thermodynamic ternary phase diagram when $\chi_{12} = 2.5$, $\chi_{13} = 3.0$, and $\chi_{23} = 3.5$. Red region indicates one phase coexistence, green region indicates two-phase coexistence, and blue region indicates three-phase coexistence. Produced by Sheng Mao from Princeton University.

what the thermodynamic triangle looked like, it was important to see if, kinetically, our system would observe the same number of phases for a given concentration on our thermodynamic phase triangle.

### 3.1.2 Kinetic Results

We assigned RGB colors to each pure component. $c_1$ is denoted with red, $c_2$ with green, and $c_3$ with blue. This can be seen in Figure 3.2 (left), which was to be used as reference in conjunction with the ternary phase triangle in Figure 3.2 (right). Every single point in the interior of the triangle corresponds to a concentration of each

component, whoch can be shown by drawing a line to the edges of the triangle like in Figure 3.3.

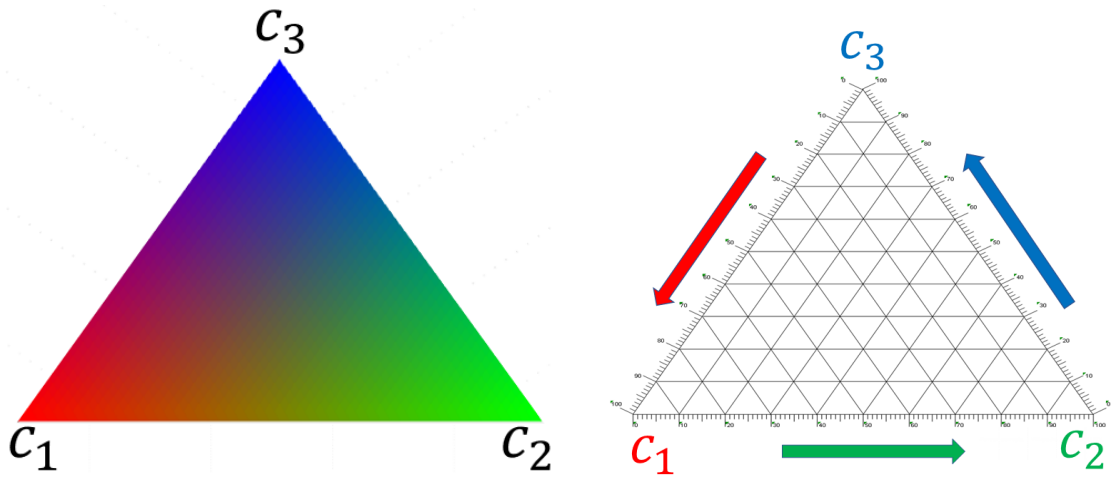


**Figure 3.2:** Left is a reference RGB triangle for the different components used in ternary system. Right adapted from https://commons.wikimedia.org/wiki/File:Ternary_plot_1.png. Arrows point toward increasing concentration on the axis of the component with the matching color.

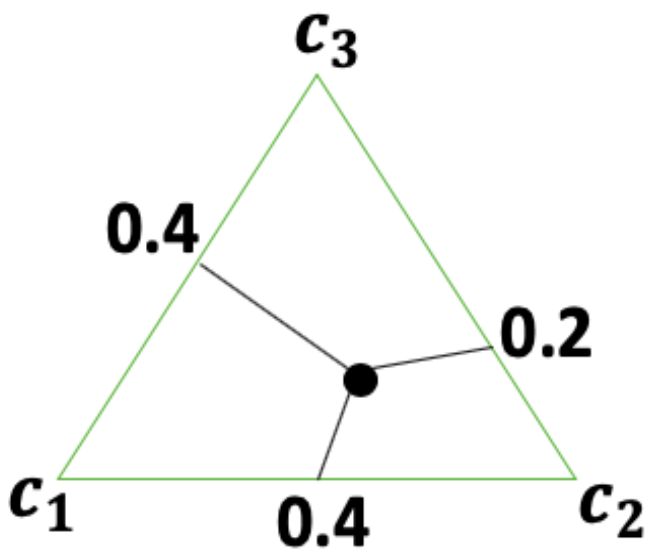


**Figure 3.3:** All interior points correspond to a concentration profile. In this example, the interior point corresponds to a concentration of 0.4 $c_1$, 0.4 $c_2$, and 0.2 $c_3$.

By running simulations for our 3-component system, the final configurations were studied and observed at different initial concentrations, eventually enabling us to construct a kinetic phase triangle, as shown in Figure 3.4(a). We defined the concentra-

tions of all three components by varying two parameters $\sigma$ and $\omega$, where $\{\sigma, \omega\} \in [0, 1]$:

$$\{c_1, c_2, c_3\} = \{\sigma(1-\omega), (1-\sigma)(1-\omega), \omega\}. \tag{3.2}$$

It is trivial to verify that $1 = \sigma(1-\omega) + (1-\sigma)(1-\omega) + \omega = c_1 + c_2 + c_3$. We prescribed values for $\omega$ and $\sigma$:

$$\omega = \{0.05, 0.1, 0.2, 0.25, 0.34, 0.4, 0.5, 0.6, 0.7, 0.8, 0.9\}, \tag{3.3}$$

$$\sigma = \begin{cases} \{0.1, 0.2, 0.3, 0.4, 0.5, 0.6, 0.7, 0.8, 0.9\} & \text{if } \omega \leq 0.6, \\ \{0.2, 0.3, 0.4, 0.5, 0.6, 0.7, 0.8\} & \text{if } 0.7 \leq \omega \leq 0.8, \\ \{0.35, 0.4, 0.45, 0.5, 0.55, 0.6, 0.65\} & \text{if } \omega = 0.9. \end{cases} \tag{3.4}$$

Having defined our concentrations, we were able to run simulations with different initial concentrations, view the phase equilibria, and create the kinetic phase diagram. As we can see in Figure 3.4(a), the three-phase region represented by white dots has shrunk into only a small subsection of the theoretical three-phase region, while the one- and two-phase regions have increased in size. This finding is particularly interesting as it draws attention to the fact if we do not wait for a system to go to equilibrium, we cannot accurately predict the number of phases we will see soley from equilibrium thermodynamics. This is very relevant in biological systems, where time scales of events do matter, such as protein folding [32], and thermodynamic equilibrium is not always reached. When thermodynamic equilibrium is not reached, understanding the kinetics of the dynamics involved with phase equilibria becomes increasingly important. Understanding of the temporal dynamics would require the construction of kinetic phase diagrams as the systems evolves in time. Kinetic diagrams would be crucial for quantitatively assessing how the three-phase region changes as the interaction parameters are altered and as the systems settles closer to equilibrium. This kind of analysis would also prove beneficial in uncovering where to observe N-phase coexistence in an N-component system. For illustration purposes, nine points, three for the three-phase, two-phase, and one-phase regions each, were selected (as indicated in Figure 3.4(b)) and the phase plots of their final configurations are shown in Figure 3.5.

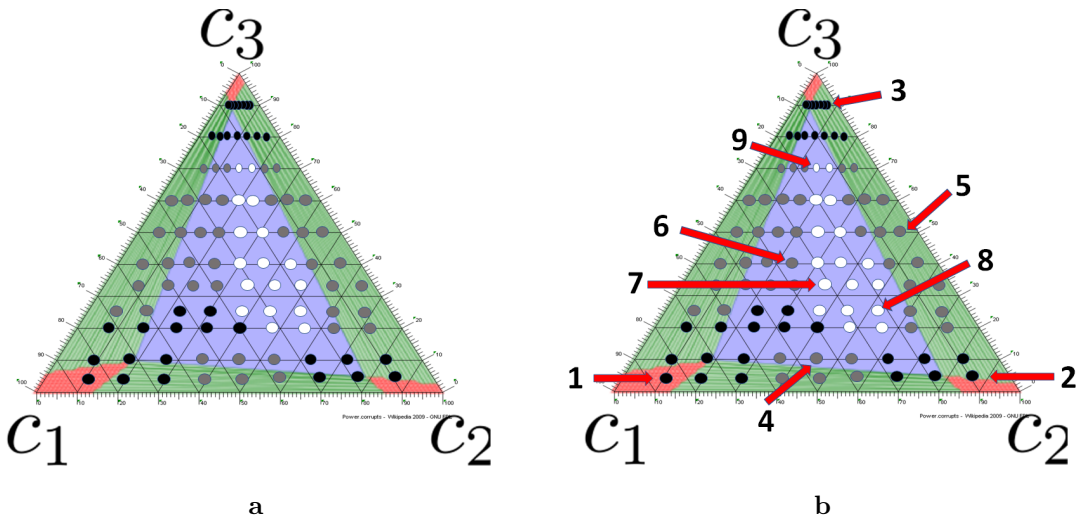


**Figure 3.4:** **a**: Kinetic ternary phase diagram when $\chi_{12} = 2.5$, $\chi_{13} = 3.0$, and $\chi_{23} = 3.5$. Red region indicates theoretical one-phase coexistence, green region indicates theoretical two-phase coexistence, and blue region indicates theoretical three-phase coexistence. Meanwhile, the black dots indicate the observed one-phase coexistence, gray dots indicate observed two-phase coexistence, and white dots indicate observed three-phase coexistence. **b**: Selected points that are displayed in Figure 3.4.

### 3.1.3 Stability Analysis

One of our main goals from this project is to generalize our results and understand how we can predict phase equilibria behavior in an N-component system. One prediction of interest is being able to predict when one will observe N-phases with an N-component mixture. This can be done using a stability analysis of the free energy of the system. More specifically, we must calculate and analyze the eigenvalues of the Hessian matrix of the free energy, computed with respect to the concentrations of each component. For the ternary system, our Hessian matrix will be a 2x2 symmetric matrix since there are only two independent variables due to the constraint $c_1 + c_2 + c_3 = 1$; thus, defining two concentrations is enough to define all three. If both eigenvalues are positive at a particular concentration set $\{c_1, c_2, c_3\}$, the Hessian matrix is positive definite, meaning that the free energy is at a local minimum at that concentration and changing to a different concentration set will raise the free energy of the system. The system is stable at this point, creating a one-phase region. Having one negative eigenvalue means that the Hessian has a saddle point at prescribed concentration set and the free energy is at a stationary point that can be easily perturbed. Hence, the free energy is likely to separate out into an additional phase, creating the two-phase region. If the Hessian has two negative eigenvalues, the free energy is at a maximum and the system will have to phase separate into three phases to lower its energy, indicating the three-phase region [27]. A similar ternary diagram plot was

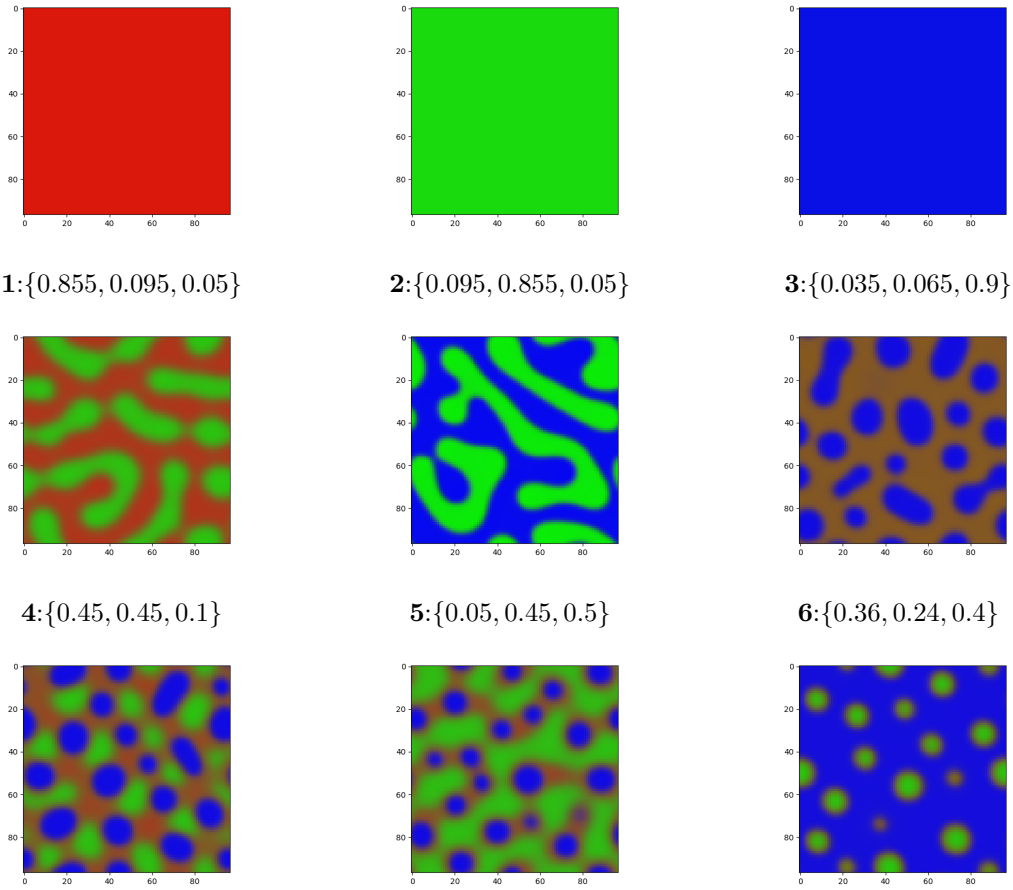

**1**:$\{0.855, 0.095, 0.05\}$ **2**:$\{0.095, 0.855, 0.05\}$ **3**:$\{0.035, 0.065, 0.9\}$

**4**:$\{0.45, 0.45, 0.1\}$ **5**:$\{0.05, 0.45, 0.5\}$ **6**:$\{0.36, 0.24, 0.4\}$

**7**:$\{0.33, 0.33, 0.34\}$ **8**:$\{0.3, 0.45, 0.25\}$ **9**:$\{0.15, 0.15, 0.7\}$

**Figure 3.5:** Phase diagrams for the ternary case when $\chi_{12} = 2.5$, $\chi_{13} = 3.0$, and $\chi_{23} = 3.5$ that correspond to the labels in Figure 3.3(b). Numbers in curly brackets are concentrations of $c_1$, $c_2$, and $c_3$, respectively. Top row is one-phase region. Middle row is two-phase region. Bottom row is three-phase region.

made in MATLAB, assigning spots on the triangle that corresponded to one-, two-, or three-phase regions based on whether the initial concentration values resulted in a Hessian matrix with two, one, or zero positive eigenvalues. Figure 3.6 displays the eigenvalue ternary phase triangle. We see in Figure 3.6 that the one- and two-phase regions roughly correspond to the one- and two-phase regions in Figure 3.4(a). However, there is no three-phase region. It has become a two phase region as well. This is peculiar as the thermodynamic and kinetic triangles from Figures 3.1 and 3.4(a) both indicate a three-phase coexistence region for this ternary system. Perhaps the eigenvalue analysis is indicative of the initial kinetics of the system. For instance, according to our thermodynamic and kinetic triangles, we expect to see three phases when $\{c_1, c_2, c_3\} = \{1/3, 1/3, 1/3\}$. However, we only see two phases according to

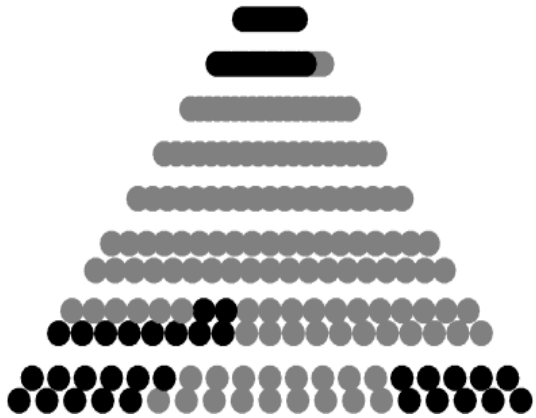

**Figure 3.6:** Kinetic ternary phase diagram created from eigenvalues of the Hessian matrix when $\chi_{12} = 2.5$, $\chi_{13} = 3.0$, and $\chi_{23} = 3.5$ at various compositions. The black dots indicate the concentrations that give rise to two positive eigenvalues, indicating that those correspond to one-phase coexistence. The gray dots indicate the concentrations that give rise to one positive eigenvalue, indicating that those correspond to two-phase coexistence..

Figure 3.6. This may suggest that, initially, the system separates into two distinct phases. Then, one of those phases separates into two additional phases at a later time when the dynamics have changed. While this behavior is hard to indicate on the time evolution of the ternary system (not shown here), the explanation that the stability analysis reveals the initial kinetics of the system is plausible and is supported by our results obtained in the quaternary component case, which will be discussed more in depth in Section 3.2.

## 3.2 Quaternary System

For the 4-component system, the free energy density took the form

$$f(c_1, c_2, c_3, c_4) = \sum_{i=1}^{4} c_i \ln(c_i) + \sum_{i<j} \chi_{ij} c_i c_j - \frac{1}{2}\lambda^2 \sum_{i<j} \chi_{ij} \nabla c_i \cdot \nabla c_j, \tag{3.5}$$

keeping in mind that the free energy density is only a function of three independent variables, $\{c_1, c_2, c_3\}$, with $c_4 = 1 - c_1 - c_2 - c_3$. Here, $c_1$, $c_2$, and $c_3$ still correspond to red, green, and blue in our phase plots. In addition, $c_4$ is represented by black. We investigated four different cases by varying the interaction parameters. This parameters are tabulated in Table 3.2. For simplicity, we kept the concentrations of all four components to be equal. Our aim was to compare how the kinetics and final configurations of each case compared with each other. Case 1 is our test case where

all interactions, which should give rise to four phases. Its evolution at different time points are displayed in Figure 3.7.

**Table 3.2:** Interaction parameters used in equimolar quaternary system.

| | **Case 1** | **Case 2** | **Case 3** | **Case 4** |
|---|---|---|---|---|
| $\chi_{12}$ | 4.2 | 3.0 | 4.0 | 3.0 |
| $\chi_{13}$ | 4.2 | 3.0 | 4.0 | 3.5 |
| $\chi_{14}$ | 4.2 | 3.5 | 3.5 | 4.0 |
| $\chi_{23}$ | 4.2 | 3.5 | 3.5 | 4.0 |
| $\chi_{24}$ | 4.2 | 4.0 | 3.0 | 3.5 |
| $\chi_{34}$ | 4.2 | 4.0 | 3.0 | 3.0 |
| $\lambda$ | $2{\cdot}10^{-5}$ | $2{\cdot}10^{-5}$ | $2{\cdot}10^{-5}$ | $2{\cdot}10^{-5}$ |

First, we begin with one phase. Then, we suddenly get the appearance of each component emerge from the initial uniform phase. Eventually, once the dynamics relax, we have four phases. To verify if we expect to get four phases, the eigenvalues of the Hessian of the free energy density were calculated for $\{c_1, c_2, c_3, c_4\} = \{0.25, 0.25, 0.25, 0.25\}$ and at the interaction parameters indicated for Case 1 in Table 3.2. The Hessian matrix indeed has three negative eigenvalues, which is what we would expect for a four component system to show four coexisting phases. Next, we

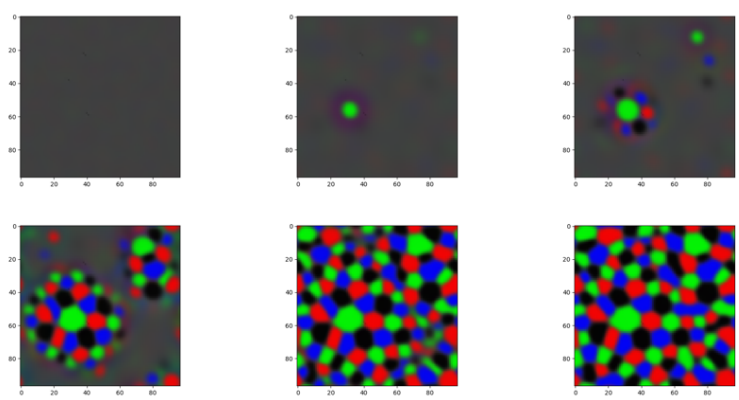

**Figure 3.7:** Evolution of Quaternary Case 1 in Table 3.2. Top row: Snapshots at 10 time steps, 300 steps, and 350 steps. Bottom row: Snapshots at 400 steps, 450 steps, and 500 steps. All time steps are $10^{-4}$ seconds.

looked at Cases 2 and 3, which were very similar as we simply switched the roles of components $c_1$ and $c_4$ by inverting the order of the interaction parameters. The phase plots showing their time evolution are shown in Figure 3.8.

For both cases, we initially see one phase in the very beginning, then we have the development of two phases, a bulk phase and a minor phase that forms droplets. Eventually, the remaining phases form from the initial bulk phase. Thus, at the end of

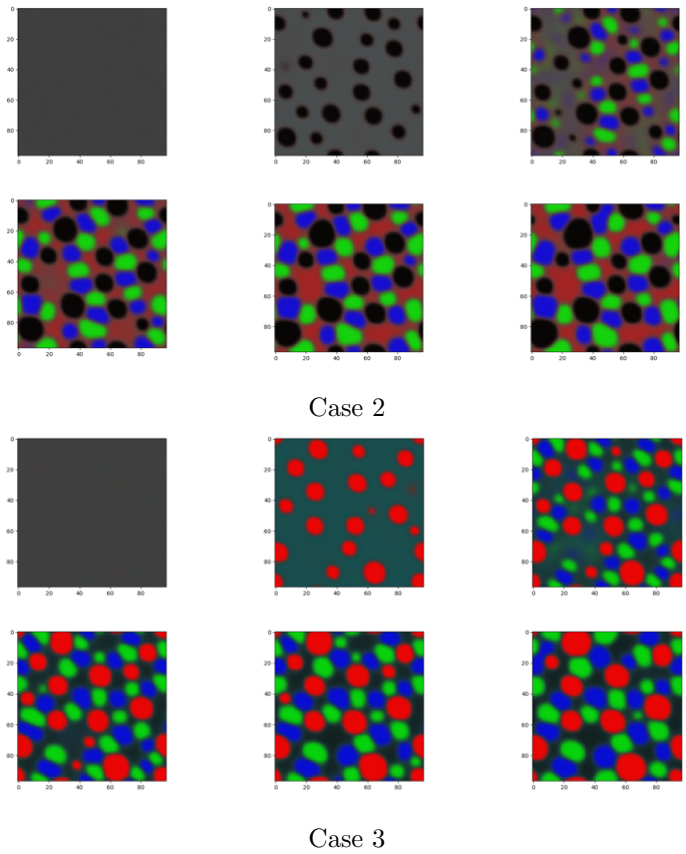


**Figure 3.8:** Evolution of Quaternary Cases 2 and 3 in Table 3.2. For both cases, the top row corresponds to number of time time steps: 10, 350, 700, the bottom row corresponds to number of time steps: 1000, 1500, 2000. Time step are $10^{-4}$ seconds.

the dynamics, we do see four separate phases such as in the equal concentration case, Case 1, though the final configurations do not take the same morphologies. Naturally, it is crucial to check the eigenvalues of the Hessian for Cases 2 and 3. Both have only one eigenvalue, indicating that only two phases will coexist at equal concentration at the prescribed interaction values. However, we do see four coexisting phases by letting the system evolve. This is similar to the phenomenon we saw with the ternary case. Here, in the beginning, we initially do have two phases that coexist for a period of time, then, the remaining phases form. This is support that the eigenvalue analysis is telling of how many coexisting phases there are for the initial state of the system, but not for the later dynamics.

Lastly, Case 4 was subjected to the same analysis. Figure 3.9 also shows its dynamics via phase plots. Initially, there are two phases as well, then eventually, each phase gives rise to two separate phases. Then the phases tend to equilibrate and spread out, eventually ending in four distinct phases. Based on the results of

Case 2 and Case 3, we should expect the Hessian matrix to have only one negative eigenvalue, corresponding to the initial two phases that exist at the beginning of the system dynamics. This is indeed what we observe. Thus, through analysis of the four component cases, we see that the eigenvalues of the Hessian matrix provide information of the phase coexistence when system dynamics have begun, but is not informative of how many phases will coexist later on when the system has evolved further. Generalizing this result to N components will be fairly easy as one only needs to observe the initial dynamics of an N component system and evaluate the corresponding free energy Hessian matrix.

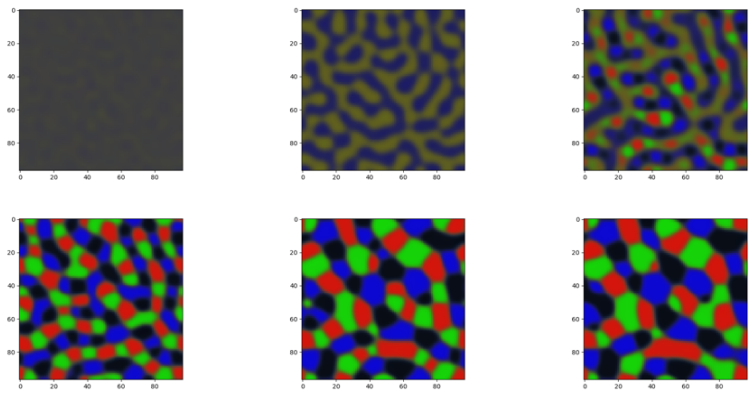

**Figure 3.9:** Evolution of Quaternary Case 4 in Table 3.2. Top row: Snapshots at 10 time steps, 100 steps, and 250 steps. Bottom row: Snapshots at 550 steps, 1500 steps, and 2000 steps. All time steps are $10^{-4}$ seconds.

# Chapter 4

# Conclusions and Future Work

During our study of the ternary system, we learned that the kinetic phase diagram constructed from our simulations does not match the thermodynamic phase diagram. This result revealed that kinetics of a system matter in addition to its behavior at thermodynamic equilibrium. Knowledge of how each region in the phase diagram changes kinetically provides information on how a thermodynamic system will evolve when equilibrium occurs too slowly in the time period of interest, such as many biological systems. By analyzing quaternary mixtures, we also learned that the eigenvalue stability analysis only provides information of coexisting phases for the initial dynamics, a result that can easily be verified in higher order mixtures.

In this report, the final morphologies observed were analyzed qualitatively. For example, it was easy to see that Cases 1 through 4 for the quaternary mixture looked different when the systems were allowed to evolve. However, these differences were not quantitatively analyzed. In the future, a more quantitative method for assessing the final morphologies of the different phases we see from our phase diagrams must be developed differentiate and categorize systems with various interaction parameters and compositions as they evolve in time. Development of a more quantitative method will be useful for studying real systems in three dimensions, where the morphologies become even more complicated with an additional degree of freedom. For instance, in addition to the morphologies observed in this report, the different components can pack in spherical or ellipsoidal compartments in three dimensions, a phenomenon observed in Feric et al. [13]. Additionally, a systematic method for uncovering how an N-phase coexistence region would evolve for different systems with N components must be developed, a feat that may be accomplished by investigating other mathematical properties of the free energy and other characteristic equations of the system.

# Bibliography


[1] M. Y. Boyarsky and A. Semenov, "Multicomponent systems thermodynamics,"

[2] G. Antonoff, "What is a phase?," *Journal of Chemical Education*, vol. 21, no. 4, p. 195, 1944.

[3] B. Cantor, I. Chang, P. Knight, and A. Vincent, "Microstructural development in equiatomic multicomponent alloys," *Materials Science and Engineering: A*, vol. 375, pp. 213–218, 2004.

[4] G. Ryan, A. Pandit, and D. P. Apatsidis, "Fabrication methods of porous metals for use in orthopaedic applications," *Biomaterials*, vol. 27, no. 13, pp. 2651–2670, 2006.

[5] C. P. Brangwynne, T. J. Mitchison, and A. A. Hyman, "Active liquid-like behavior of nucleoli determines their size and shape in xenopus laevis oocytes," *Proceedings of the National Academy of Sciences*, vol. 108, no. 11, pp. 4334–4339, 2011.

[6] A. Patel, H. O. Lee, L. Jawerth, S. Maharana, M. Jahnel, M. Y. Hein, S. Stoynov, J. Mahamid, S. Saha, T. M. Franzmann, *et al.*, "A liquid-to-solid phase transition of the als protein fus accelerated by disease mutation," *Cell*, vol. 162, no. 5, pp. 1066–1077, 2015.

[7] J. M. Sanchez, F. Ducastelle, and D. Gratias, "Generalized cluster description of multicomponent systems," *Physica A: Statistical Mechanics and its Applications*, vol. 128, no. 1-2, pp. 334–350, 1984.

[8] K. Binder and D. Stauffer, "Theory for the slowing down of the relaxation and spinodal decomposition of binary mixtures," *Physical Review Letters*, vol. 33, no. 17, p. 1006, 1974.

[9] K. Binder, C. Billotet, and P. Mirold, "On the theory of spinodal decomposition in solid and liquid binary mixtures," *Zeitschrift für Physik B Condensed Matter*, vol. 30, no. 2, pp. 183–195, 1978.

[10] J. Jenkins and F. Mancini, "Kinetic theory for binary mixtures of smooth, nearly elastic spheres," *Physics of Fluids A: Fluid Dynamics*, vol. 1, no. 12, pp. 2050–2057, 1989.

[11] A. Matsuyama and T. Kato, "Theory of binary mixtures of a flexible polymer and a liquid crystal," *The Journal of chemical physics*, vol. 105, no. 4, pp. 1654–1660, 1996.

[12] L.-S. Luo and S. S. Girimaji, "Theory of the lattice boltzmann method: two-fluid model for binary mixtures," *Physical Review E*, vol. 67, no. 3, p. 036302, 2003.

[13] M. Feric, N. Vaidya, T. S. Harmon, D. M. Mitrea, L. Zhu, T. M. Richardson, R. W. Kriwacki, R. V. Pappu, and C. P. Brangwynne, "Coexisting liquid phases underlie nucleolar subcompartments," *Cell*, vol. 165, no. 7, pp. 1686–1697, 2016.

[14] A. Z. Panagiotopoulos, *Essential Thermodynamics*. Drios Press, 2014.

[15] C. D. Stoner, "Inquiries into the nature of free energy and entropy in respect to biochemical thermodynamics," *Entropy*, vol. 2, no. 3, pp. 106–141, 2000.

[16] K. Dill and S. Bromberg, *Molecular Driving Forces: Statistical Thermodynamics in Biology, Chemistry, Physics, and Nanoscience*. Garland Science, 2010.

[17] P. J. Flory, "Thermodynamics of high polymer solutions," *The Journal of chemical physics*, vol. 10, no. 1, pp. 51–61, 1942.

[18] M. L. Huggins, "Solutions of long chain compounds," *The Journal of chemical physics*, vol. 9, no. 5, pp. 440–440, 1941.

[19] M. Rubenstein and R. Colby, *Polymer Physics*. Oxford University Press, 2003.

[20] B. Predel, M. Hoch, and M. J. Pool, *Phase Diagrams and Heterogeneous Equilibria: a Practical Introduction*. Springer Science & Business Media, 2013.

[21] J. Berry, C. Brangwynne, and M. P. Haataja, "Physical principles of intracellular organization via active and passive phase transitions," *Reports on Progress in Physics*, 2018.

[22] R. J. LeVeque, *Finite Difference Methods for Ordinary and Partial Differential Equations: Steady-state and Time-dependent Problems*, vol. 98. Siam, 2007.

[23] J. N. Reddy, *An Introduction to the Finite Element Method*, vol. 2. McGraw-Hill New York, 1993.

[24] H. P. Langtangen, "A fenics tutorial," in *Automated Solution of Differential Equations by the Finite Element Method*, pp. 1–73, Springer, 2012.

[25] R. Haberman, *Elementary Applied Partial Differential Equations*, vol. 987. Prentice Hall Englewood Cliffs, NJ, 1983.

[26] T. Cebeci, *Convective heat transfer*. Springer, 2002.

[27] R. Larson and B. H. Edwards, *Calculus*. Cengage Learning, 2009.

[28] J. W. Cahn and J. E. Hilliard, "Free energy of a nonuniform system. i. interfacial free energy," *The Journal of chemical physics*, vol. 28, no. 2, pp. 258–267, 1958.

[29] C. Lanczos, *The Variational Principles of Mechanics*. Courier Corporation, 2012.

[30] G. Voronin and A. Voskov, "Calculation of phase equilibria and construction of phase diagrams by convex hull method," *Moscow University Chemistry Bulletin*, vol. 68, no. 1, pp. 1–8, 2013.

[31] E. K. Chong and S. H. Zak, *An introduction to optimization*, vol. 76. John Wiley & Sons, 2013.

[32] J. D. Bryngelson and P. G. Wolynes, "Spin glasses and the statistical mechanics of protein folding," *Proceedings of the National Academy of Sciences*, vol. 84, no. 21, pp. 7524–7528, 1987.